Highly Efficient Midinfrared On-Chip Electrical Generation of Graphene Plasmons by Inelastic Electron Tunneling Excitation

Kelvin J. A. Ooi,[1,*] H. S. Chu,[2,*] C. Y. Hsieh,[1,3] Dawn T. H. Tan,[1] and L. K. Ang[1]

[1]*Engineering Product Development, Singapore University of Technology and Design,*
East Coast Campus, 8 Somapah Road, Singapore 487372, Singapore
[2]*Electronics & Photonics Department, A*STAR Institute of High Performance Computing,*
1 Fusionopolis Way, #16-16 Connexis, Singapore 138632, Singapore
[3]*Department of Chemistry, Massachusetts Institute of Technology, Cambridge, Massachusetts 02139, USA*

Inelastic electron tunneling provides a low-energy pathway for the excitation of surface plasmons and light emission. We theoretically investigate tunnel junctions based on metals and graphene. We show that graphene is potentially a highly efficient material for tunneling excitation of plasmons because of its narrow plasmon linewidths, strong emission, and large tunability in the midinfrared wavelength regime. Compared to gold and silver, the enhancement can be up to 10 times for similar wavelengths and up to 5 orders at their respective plasmon operating wavelengths. Tunneling excitation of graphene plasmons promises an efficient technology for on-chip electrical generation and manipulation of plasmons for graphene-based optoelectronics and nanophotonic integrated circuits.

I. INTRODUCTION

In 1976, Lambe and McCarthy [1] discovered light emission from metal-insulator-metal (M-I-M) tunnel junctions. Following the discovery, light-emitting tunnel junctions had drawn research interest in both theory and experiment to understand the emission process [2–5]. The consensus in those papers is that the light emission is plasmon mediated. Recently, there are renewed interests in the tunnel junction as surface-plasmon sources [6–11]. One advantage of having surface-plasmon tunnel junctions (SPTJs) is the *in situ* generation of surface plasmons avoiding the need for free-space optical couplings, which are often bulky and inefficient. Another advantage of SPTJs is the low-energy excitation compared to other higher-energy excitation pathways like electron bombardment or aloof scattering [12–14].

Existing light-emitting tunnel junctions and SPTJs use metals as the tunnel-junction electrodes, in particular, aluminum, silver, and gold [2–11]. In this paper, we theoretically study graphene as a material for the tunneling excitation of surface plasmons. Most of the current research on graphene tunnel junctions shows that inelastic electron tunneling occurs mainly through phonon channels [15–17]. However, inelastic electron tunneling through plasmon channels has also been experimentally demonstrated [15]. We show that because of graphene's narrow plasmon linewidths and SPPs operating in the midinfrared

wavelength regime, the inelastic electron tunneling excitation of graphene plasmons will be much more efficient compared to most metals.

The prevailing theory for the inelastic electron tunneling plasmon (IETP) excitation mechanism is that at low bias voltages, it occurs through a three-step process [5–11]: (i) electrons tunnel inelastically from one electrode to another in a M-I-M junction, (ii) gap plasmons are excited through coupling from the energy loss $\hbar\omega$, and (iii) gap plasmons are coupled out to surface-plasmon polaritons (SPPs) and then into radiation.

Hence, we investigate IETP excitation using a two-part approach: In the first part, we study the frequency-dependent gap-plasmon formation from IETP excitation using available formulations [2]. Then, in the second part, we perform the finite-difference time-domain (FDTD) simulations by means of the Lumerical commercial software [18] to find the coupling efficiency of gap plasmons into SPPs. The final result is obtained by superimposing the optical power spectrum from both parts. Our approach can fairly reproduce some of the spectral features from previous IETP excitation experiments [4,6,10].

II. THEORY OF GAP-PLASMON EXCITATION FROM INELASTIC ELECTRON TUNNELING

A. Gap plasmons in M-I-M tunnel junctions

To find the gap-plasmon power spectrum, first we need to find the tunneling currents and induced gap-plasmon electric fields. The formulation for a M-I-M tunnel junction depicted in Fig. 1(a) can be found in Ref. [2] but will be briefly reproduced here. The tunneling current is written as

*Corresponding author.
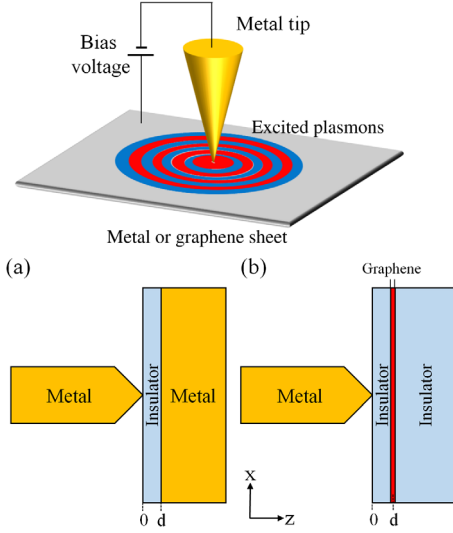kelvin_ooi@sutd.edu.sg
chuhs@ihpc.a-star.edu.sg

FIG. 1. Schematic of the plasmon excitation from a metal-insulator-metal or -graphene tunnel junction. (a) Metal-insulator-metal tunnel junction. (b) Metal-insulator-graphene tunnel junction.

$$J = \left(\frac{ie\hbar}{2m_e^*}\right)(\psi_R^* \nabla\psi_L - \psi_L \nabla\psi_R^*), \tag{1}$$

where ψ is the electronic wave function on the left (L) and right (R) electrodes and is described by

$$\psi_L = \frac{1}{\sqrt{2Al}}\chi_L \exp(-iE_L t/\hbar), \tag{2a}$$

$$\psi_R = \frac{1}{\sqrt{2Al}}\chi_R \exp(-i[qx + E_R t/\hbar]), \tag{2b}$$

where A and l are the normalization of the area and length of the electrodes, respectively, E is the energy of the electrodes, q is the plasmon vector, and χ is the eigenfunction given by [19]

$$\chi_L = \begin{cases} e^{ik_L z} + R_L e^{-ik_L z}, & z < 0, \\ C_L e^{-K_L z} + D_L e^{K_L z}, & 0 < z < d, \\ T_L e^{ik_L(z-d)}, & d < z, \end{cases} \tag{2c}$$

$$\chi_R = \begin{cases} T_R e^{-ik_R z}, & z < 0, \\ C_R e^{-K_R(d-z)} + D_R e^{K_R(d-z)}, & 0 < z < d, \\ e^{-ik_R(z-d)} + R_R e^{-ik_R(z-d)}, & d < z, \end{cases} \tag{2d}$$

where R, C, D, and T are the coefficients found from the boundary conditions such that χ and $d\chi/dz$ are continuous at $z = 0$ and $z = d$. The eigenfunctions carry the momentum terms

$$k_L = (2m_e^* E_L/\hbar^2)^{1/2}, \tag{3a}$$

$$K_L = [2m_e^*(U_0 - E_L)/\hbar^2]^{1/2}, \tag{3b}$$

$$k_R = (2m_e^* E_R/\hbar^2 - q^2)^{1/2}, \tag{3c}$$

$$K_R = [2m_e^*(U_0 - E_R)/\hbar^2 + q^2]^{1/2}, \tag{3d}$$

where U_0 is the barrier height of the emitting left electrode, and m_e^* is the effective electron mass.

Figure 2(a) depicts the inelastic electron tunneling process used to generate plasmons. In the equilibrium state, E_L and E_R align at the same Fermi level. On the application of a bias voltage across the *M-I-M* junction, the energy levels shift, and the difference in Fermi level drives the tunneling currents and then excites the gap plasmon, with energy $E_L - E_R = \hbar\omega$. The cutoff frequency is determined by the applied bias voltage, $\hbar\omega = eV_z$ [1].

Then, the induced electric fields arising from the transition charges can be simply found from Gauss's law

$$\nabla \cdot \left[\varepsilon_{(z,\omega)} \nabla\varphi\right] = 4\pi\rho_z, \tag{4}$$

where ε is the permittivity of the material which is dependent on frequency ω and location z, $\rho = -e\psi_L \psi_R^*$
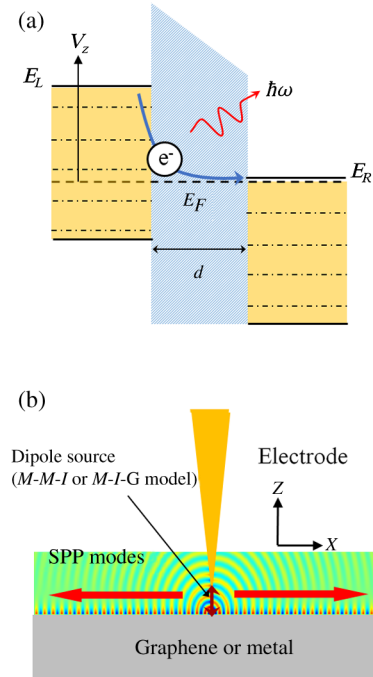

FIG. 2. (a) Mechanism of the inelastic electron tunneling in generating a gap plasmon. Upon applying a bias voltage V_z, the energy level of the left electrode is shifted and electrons tunnel inelastically to the right electrode, exciting a gap plasmon with energy $\hbar\omega = eV_z$. (b) Model of the 2D FDTD simulation. The gap-plasmon mode is modeled as a line dipole source with a normalized power of 1 W at all wavelengths. The power is coupled out as SPP modes and propagates along the metal or graphene surface.

is the charge density distribution, and $\boldsymbol{F} = -\boldsymbol{\nabla}\varphi$ is the electric field. Finally, the gap-plasmon power can be obtained from the equation

$$P_{\text{gap plasmon}} = -2\text{Re} \int \boldsymbol{F}^* \cdot \boldsymbol{J} dz. \tag{5}$$

Next, the surface-plasmon spectrum can be obtained by defining a frequency-dependent q, which is obtained from the surface-plasmon dispersion curve for M-I-M structures given by

$$(\varepsilon_L + \varepsilon_0)(\varepsilon_R + \varepsilon_0) - (\varepsilon_L - \varepsilon_0)(\varepsilon_R - \varepsilon_0)\exp(-2qd) = 0, \tag{6}$$

where ε_L, ε_R, and ε_0 are the permittivity for the left and right electrodes and the gap, respectively.

B. Gap plasmons in M-I-G tunnel junctions

The development of the theoretical formulation of the graphene IETP system is similar to the ones described from the previous section but with a few modifications. First, there is a tunneling electron mass anisotropy in graphene [20], where the out-of-plane mass $m_\perp = m_e$ is normal while the in-plane mass is relativistic given by $m_\parallel = E_F/v_F^2$ [21], where E_F is the Fermi level of graphene and $v_F = 10^6$ m/s is the Fermi velocity. This tunneling electron mass anisotropy results in modification of the wave-function momentum terms at the right interface

$$k_R = \left(\frac{2m_\perp E_R}{\hbar^2} - \frac{m_\perp}{m_\parallel}q^2\right)^{1/2}, \tag{7a}$$

$$K_R = \left[\frac{2m_\perp(U_0 - E_R)}{\hbar^2} + \frac{m_\perp}{m_\parallel}q^2\right]^{1/2}. \tag{7b}$$

Next, as shown in Fig. 1(b), the graphene is modeled as a 2D material, and, therefore, it has an associated 2D charge density. This charge density will result in the boundary conditions for the electric fields, $\varepsilon\nabla\phi_z$ being not continuous at $z = d$.

We start by writing the solutions for the electric-potential boundary conditions

$$\varphi(z) = \begin{cases} a_L e^{qz} + g_L(z), & z < 0, \\ a_+ e^{qz} + a_- e^{-qz} + g_0(z), & 0 < z < d, \\ a_R e^{-q(z-d)} + g_R(z), & d < z, \end{cases} \tag{8}$$

where g_L, g_0, and g_R are the inhomogeneous parts of the solutions [2]. Hence, we can write the algebraic equations

$$a_L + g_L(0) = a_+ + a_- + g_0(0), \tag{9a}$$

$$a_+ e^{qd} + a_- e^{-qd} + g_0(d) = a_R + g_R(d). \tag{9b}$$

Since $\varepsilon\nabla\phi_z$ is not continuous at $z = d$, the charge-density term $i\omega\rho = \nabla J_x$ arises, and

$$\nabla J_x = \sigma\nabla^2\varphi_{(z=d)}$$
$$= -\sigma q^2\varphi_{(z=d)}, \tag{10}$$

where σ is the 2D conductivity of graphene. Thus, we write the algebraic equations for the electric fields

$$\varepsilon_L[a_L q + g_L'(0)] = \varepsilon_0[a_+ q - a_- q + g_0'(0)], \tag{11a}$$

$$\varepsilon_0[a_+ e^{qd}q - a_- e^{-qd}q + g_0'(d)]$$
$$= \varepsilon_R[-a_R q + g_R'(d)] - \frac{iq^2\sigma}{\omega}[a_+ e^{qd} + a_- e^{-qd} + g_0(d)]. \tag{11b}$$

Combining and rearranging all four equations from Eqs. (9a), (9b), (11a), and (11b), we find the coefficients

$$a_L = a_+ + a_- + g_0(0) - g_L(0), \tag{12a}$$

$$a_R = a_+ e^{qb} + a_- e^{-qb} + g_0(b) - g_R(b), \tag{12b}$$

$$a_+ = -e^{-qd}[e^{-qd}S_1(\varepsilon_R - \varepsilon_0 + iq\sigma/\omega) - S_2(\varepsilon_L + \varepsilon_0)]/\eta, \tag{12c}$$

$$a_- = e^{-qd}[e^{qd}S_1(\varepsilon_0 + \varepsilon_R + iq\sigma/\omega) - S_2(\varepsilon_L - \varepsilon_0)]/\eta, \tag{12d}$$

where

$$\eta = (\varepsilon_L + \varepsilon_0)(\varepsilon_R + \varepsilon_0 + iq\sigma/\omega)$$
$$- (\varepsilon_L - \varepsilon_0)(\varepsilon_R - \varepsilon_0 + iq\sigma/\omega)e^{-2qd}, \tag{13a}$$

$$S_1 = \varepsilon_L[g_L(0) - g_0(0)] + [\varepsilon_0 g_0'(0) - \varepsilon_L g_L'(0)]/q, \tag{13b}$$

$$S_2 = \varepsilon_R[g_R(d) - g_0(d)] + [\varepsilon_R g_R'(d) - \varepsilon_0 g_0'(d)]/q$$
$$- iq\sigma g_0(b)/\omega. \tag{13c}$$

The 2D charge density allows the formation of the gap plasmon between the graphene and the metal tip. Here, η also represents the pole of the p-polarized reflection coefficient of the M-I-G junction. Consequently, we can find the dispersion for M-I-G tunnel junctions by letting $\eta \to 0$.

III. VERIFICATION MODELS FOR EXPERIMENTAL SPPs AND EMISSION SPECTRA

Following our developed theoretical approach as stated in Secs. I and II, we try to reproduce the IETP excitation spectra from past experiments. The gap-plasmon spectrum is numerically obtained from formulations in Sec. II, while the gap plasmon to SPP coupling spectrum is obtained from Lumerical 2D FDTD simulations. In the FDTD simulation, the gap plasmon is modeled as an electric dipole source, with power normalized at 1 W at all wavelengths, connecting the emitter electrode and the metal substrate as shown in Fig. 2(b). The gap plasmons then couple to the SPP modes and propagate along the metal substrate. The SPP is allowed to propagate a few micrometers along the substrate, and then the near-field spectrum of the SPP is recorded. Superimposing both spectra results in the SPP or emission intensity spectrum.

In our first study, we simulate the intensity spectrum of an Al-Al$_2$O$_3$-Ag tunnel junction for different bias voltages as described in Ref. [4]. The complex permittivity for Al is taken from Palik's handbook [22], while that for Ag is obtained from Johnson and Christy's paper [23]. The permittivity of Al$_2$O$_3$ is approximately 3 and has an effective tunneling mass of $0.2m_e$ [24]. The results of both simulated and experimental spectra are compared in Fig. 3. We observe that the simulated results can reproduce the general shape of the spectra as well as the cutoff wavelengths of the emission. However, there are some discrepancies in the peak wavelengths, where the simulated peak

wavelength for 2.7 V is slightly redshifted (575 nm) compared to the experimental peak (540 nm). The discrepancy gets larger at higher bias voltages. The blueshift of the experimental spectra is due to the spectra being recorded in the far field, in contrast to our simulation spectra being recorded in the near field [25]. Moreover, the discrepancies can also be due to the imperfection of the fabricated structures such as surface roughness and the value of the complex permittivity used in modeling. Nevertheless, the IETP excitation theory is adequate for comparative analysis of excitation efficiencies between different plasmonic materials.

In our second study, we simulate an Au-air-Au IETP system biased at 2 V, as described in Ref. [6]. In our FDTD simulation structure, the Au tip radius is 50 nm. The permittivity of Au is obtained from Johnson and Christy [23]. The simulated spectrum in Fig. 4(a) shows that the spectrum shape and cutoff wavelength have good agreement with the experimental results from Ref. [6]. Similar to our first study, the simulated Au-air-Au IETP system has a redshifted peak wavelength (780 nm) compared to the experimental spectrum (720 nm).

Our third study consists of the same Au-air-Au IETP system but under a bias of 2.5 V. With a higher bias voltage, the peak wavelength (750 nm) of the simulated spectrum in Fig. 4(b) is shorter compared to the second study. Compared to the experimental results from Ref. [10] (700 nm), the obtained result shows a similar redshifted peak.
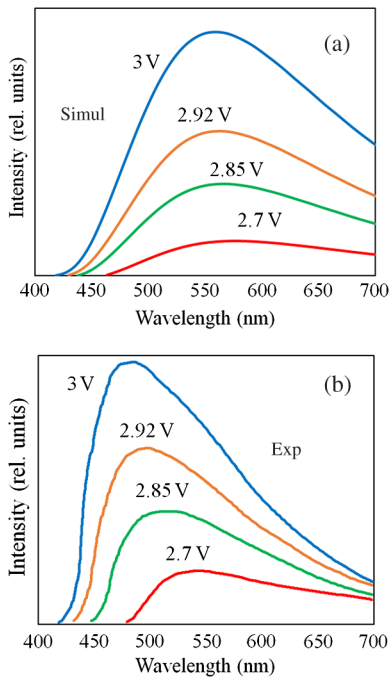

FIG. 3. Comparison of intensity spectrum of the Al-Al$_2$O$_3$-Ag IETP system: (a) simulated and (b) experimental [4].
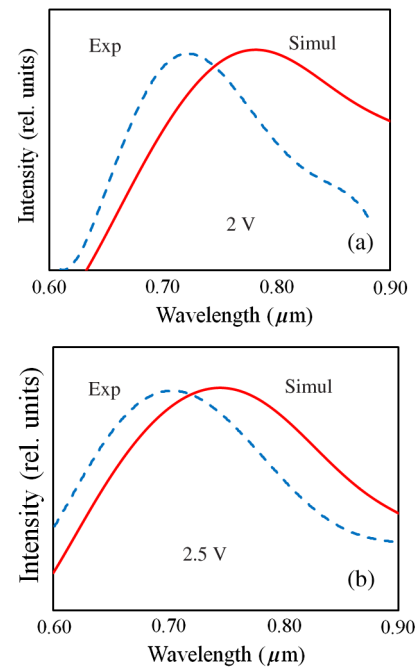

FIG. 4. Comparison of simulated (solid lines) and experimental (dashed lines) intensity spectrum of Au-air-Au IETP system under bias of (a) 2 V [6] and (b) 2.5 V [10].
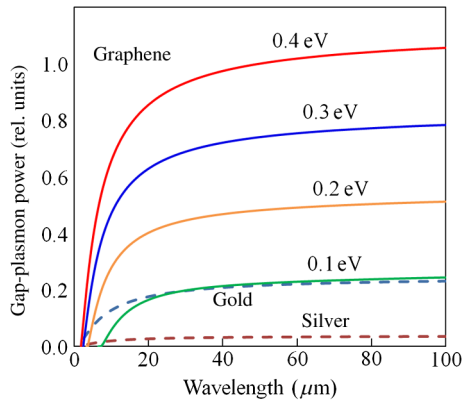
FIG. 5. IETP gap plasmons from tunneling from an aluminum tip to metals (dashed lines) and to graphene of various Fermi levels (solid lines).

IV. COMPARISON OF IETP PERFORMANCE FOR METALS AND GRAPHENE

We numerically calculate the IETP gap-plasmon power for tunnel junctions between an aluminum tip and samples consisting of metals and graphene, for a tip bias of 2 V. For metals, we select gold and silver, which have good plasmonic properties in the visible regime. While for graphene, we study the case for four doped graphene Fermi levels ranging from 0.1 to 0.4 eV. The conductivity and material parameters for graphene are taken from Ref. [26]. In all cases, a 3-nm air gap between the tip and sample ($d = 3$ nm) is chosen, and graphene is assumed to be freestanding for simplicity. From the calculated results plotted in Fig. 5, we predict that the IETP gap-plasmon power for graphene is very much larger than that for gold and silver by up to 10 times in the long wavelength

regime. The IETP gap-plasmon power rises quickly from the cutoff wavelength (defined by the lower between the tip-bias cutoff frequency and the gap-plasmon resonance frequency) and saturates at the long wavelength regime.

However, not all wavelengths support the formation and sustenance of SPPs. Full assessment of the SPP generation efficiency requires knowledge of the coupling efficiency of gap plasmons into SPPs. Here, we perform Lumerical 2D FDTD simulations of the IETP systems as depicted in Figs. 1(a) and 1(b) as a direct way to obtain the coupling efficiencies. In our simulations, we standardize the structure to be an infinitely long and straight aluminum flat tip of 20 nm width, placed 3 nm away in air from the metal and graphene substrate, as depicted in Fig. 6(a). A dipole excitation source is placed in the middle of the air gap to simulate the gap plasmon, and the outcoupled SPP power in the x direction is recorded. We find that the coupling efficiency (normalized to propagation losses) of the gap plasmons to SPPs on gold, silver, and graphene substrates is between 0.5% and 2%, as shown in Figs. 6(b)–6(d). However, the critical difference lies in their respective SPP operating wavelengths, i.e., gold and silver in the visible regime, and graphene in the midinfrared regime. Importantly, if we also take the gap-plasmon generation efficiency into account [by superimposing Figs. 6(b)–6(d) with Fig. 5], we find that the total generation efficiency of graphene SPPs greatly surpasses that of gold and silver by 5–6 orders, as shown in Figs. 6(e)–6(g).

There are at least two reasons why the IETP efficiency of graphene plasmons is greater than that of metal plasmons. The first reason, as stated before, is the different operating wavelength regimes. It is easier for electrons to lose energy inelastically through lower plasmon momentum channels compared to higher ones.
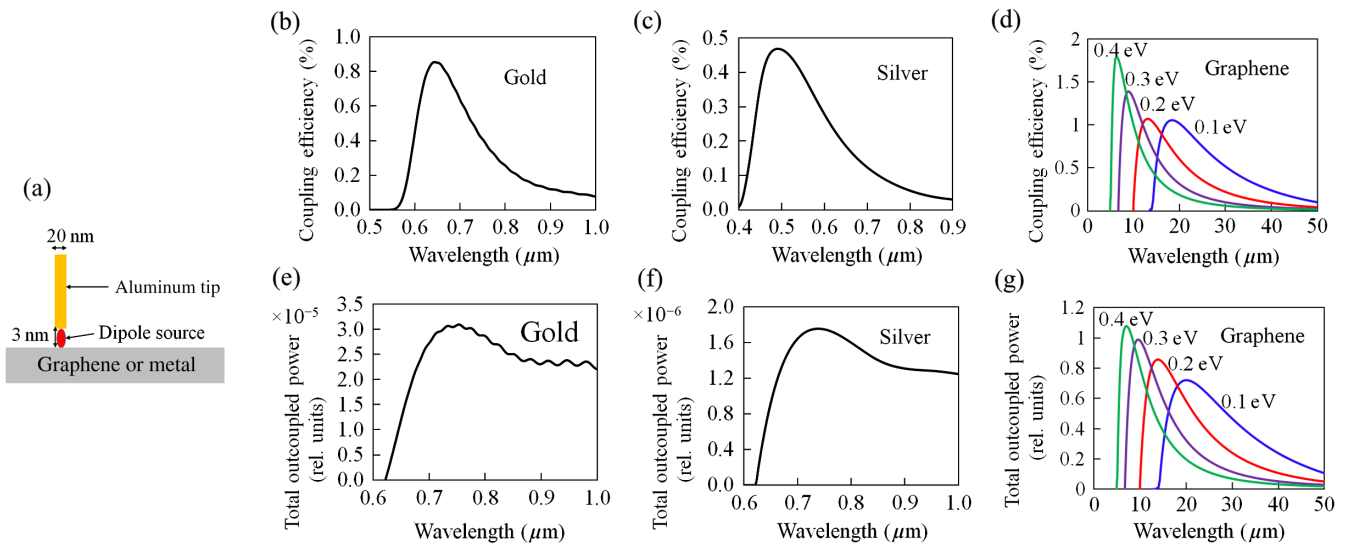

FIG. 6. (a) Schematic of the FDTD electromagnetic simulation structure. (b),(c),(d) are coupling efficiencies of gap plasmons to gold, silver, and graphene substrates, respectively. (e),(f),(g) are the total efficiencies in generating SPPs in gold, silver, and graphene, respectively.
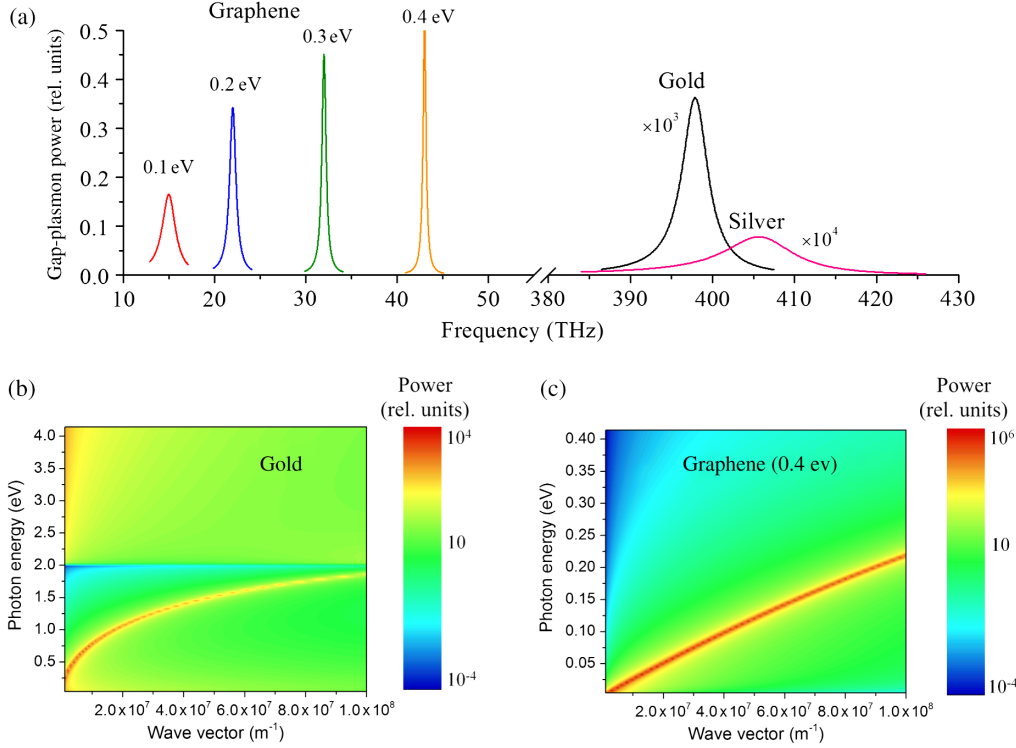
FIG. 7. (a) Frequency linewidths for the gap plasmons for graphene, gold, and silver. Graphene gap plasmons have narrower linewidths compared to metal gap plasmons. (b) and (c) are gap-plasmon power plots for each plasmon vector q and photon energy in eV, for gold and 0.4-eV graphene, respectively. The gap-plasmon power for graphene is more confined along the plasmon dispersion curve compared to gold. These results show that graphene exhibits a much larger Q factor and is tuneable compared to gold and silver materials.

The second reason can be attributed to the narrow linewidths of the generated graphene plasmons. To examine the plasmon linewidths, we selecte the plasmon vector q associated with the peak wavelengths from Figs. 6(e)–6(g). Then, using the selected q, we plot out the frequency linewidths in Fig. 7(a). We observe that the frequency linewidths for graphene gap plasmons is small, with a FWHM in the range of 1–2 THz, compared to the larger linewidths for gold and silver, with a FWHM in the range of 4–10 THz. We also plot out the gap-plasmon power for gold and 0.4-eV graphene, in Figs. 7(b) and 7(c), respectively, for each plasmon vector q and photon energy. We see that the energy spread for graphene gap plasmons is smaller, contributing to a higher peak energy along the plasmon dispersion curve, while for gold, the energy spread is larger, contributing to a lower peak energy. This finding demonstrates a potential direction to develop large tunability and high-Q nanoplasmonic devices based on the graphene platform for on-chip electrical-plasmon generation and manipulation.

The plasmon linewidth is partly governed by the relaxation time constant of the material τ, which is the mean free time of electronic collisions that leads to optical losses. In metals, τ is usually small, in the order of 0.01–0.1 ps [22,23], and, thus, optical losses are high. For graphene, τ is given by $\tau = \mu_e E_F / e v_F^2$ [26], where $\mu_e = 10^4$ cm^2/V s is the typical value of the carrier mobility [26,27], and, thus, τ is evaluated to be in the range of 0.1–0.4 ps for doped graphene Fermi levels from 0.1 to 0.4 eV. Hence, the optical losses and plasmon linewidth can be made smaller

with higher carrier mobilities and doping levels. Carrier mobilities are largely limited by charged-impurity scattering in the graphene sample [28]. While there are concerns that chemical doping of graphene will introduce impurities that degrade the carrier mobility, there are a few ways to overcome this. For example, molecular adsorption can act as a compensator that neutralizes the effects of the impurities [29]. On the other hand, the Fermi level of graphene can also be tuned by other methods, for example, electrostatic gating and photoinduced doping, that preserve the carrier mobility [27,30].

V. CONCLUSIONS

In conclusion, we study the IETP excitation for graphene and metals. The generation efficiency of graphene plasmons is expected to be much larger compared to metal plasmons due to the former's narrow plasmon linewidths and SPPs operating in the midinfrared wavelength regime. The IETP excitation of graphene has the potential to be an efficient and low-powered plasmon source for graphene-based optoelectronic devices, which will show great promise in developing the field of on-chip electrical-plasmon generation and manipulation for nanophotonic integrated circuits.

———

[1] J. Lambe and S. L. McCarthy, Light Emission from Inelastic Electron Tunneling, Phys. Rev. Lett. **37**, 923 (1976).

[2] L. C. Davis, Theory of surface-plasmon excitation in metal-insulator-metal tunnel junctions, Phys. Rev. B **16**, 2482 (1977).

[3] J. R. Kirtley, T. N. Theis, J. C. Tsang, and D. J. DiMaria, Hot-electron picture of light emission from tunnel junctions, Phys. Rev. B **27**, 4601 (1983).

[4] P. Dawson, D. G. Walmsley, H. A. Quinn, and A. J. L. Ferguson, Observation and explanation of light-emission spectra from statistically rough Cu, Ag, and Au tunnel junctions, Phys. Rev. B **30**, 3164 (1984).

[5] S. Ushioda, J. E. Rutledge, and R. M. Pierce, Prism-Coupled Light Emission from Tunnel Junctions, Phys. Rev. Lett. **54**, 224 (1985).

[6] P. Bharadwaj, A. Bouhelier, and L. Novotny, Electrical Excitation of Surface Plasmons, Phys. Rev. Lett. **106**, 226802 (2011).

[7] T. Wang, E. Boer-Duchemin, Y. Zhang, G. Comtet, and G. Dujardin, Excitation of propagating surface plasmons with a scanning tunnelling microscope, Nanotechnology **22**, 175201 (2011).

[8] R. Marty, C. Girard, A. Arbouet, and G. Colas des Francs, Near-field coupling of a point-like dipolar source with a thin metallic film: Implication for STM plasmon excitations, Chem. Phys. Lett. **532**, 100 (2012).

[9] E. Le Moal, S. Marguet, B. Rogez, S. Mukherjee, P. Dos Santos, E. Boer-Duchemin, G. Comtet, and G. Dujardin, An electrically excited nanoscale light source with active angular control of the emitted light, Nano Lett. **13**, 4198 (2013).

[10] Y. Zhang, E. Boer-Duchemin, T. Wang, B. Rogez, G. Comtet, E. Le Moal, G. Dujardin, A. Hohenau, C. Gruber, and J. R. Krenn, Edge scattering of surface plasmons excited by scanning tunneling microscopy, Opt. Express **21**, 13938 (2013).

[11] S. Divitt, P. Bharadwaj, and L. Novotny, The role of gap plasmons in light emission from tunnel junctions, Opt. Express **21**, 27452 (2013).

[12] R. H. Ritchie, Plasma losses by fast electrons in thin films, Phys. Rev. **106**, 874 (1957).

[13] F. J. García de Abajo, Optical excitations in electron microscopy, Rev. Mod. Phys. **82**, 209 (2010).

[14] K. J. A. Ooi, W. S. Koh, H. S. Chu, D. T. H. Tan, and L. K. Ang, Efficiencies of aloof-scattered electron beam excitation of metal and graphene plasmons, IEEE Trans. Plasma Sci. **43**, 951 (2015).

[15] L. Vitali, M. A. Schneider, K. Kern, L. Wirtz, and A. Rubio, Phonon and plasmon excitation in inelastic electron tunneling spectroscopy of graphite, Phys. Rev. B **69**, 121414(R) (2004).

[16] Y. Zhang, V. W. Brar, F. Wang, C. Girit, Y. Yayon, M. Panlasigui, A. Zettl, and M. F. Crommie, Giant phonon-induced conductance in scanning tunnelling spectroscopy of gate-tunable graphene, Nat. Phys. **4**, 627 (2008).

[17] R. Beams, P. Bharadwaj, and L. Novotny, Electroluminescence from graphene excited by electron tunnelling, Nanotechnology **25**, 055206 (2014).

[18] Lumerical Solutions, Inc., https://www.lumerical.com.

[19] A. D. Brailsford and L. C. Davis, Impurity-assisted inelastic tunneling: One-electron theory, Phys. Rev. B **2**, 1708 (1970).

[20] P. R. Wallace, The band theory of graphite, Phys. Rev. **71**, 622 (1947).

[21] V. Ariel and A. Natan, in *Proceedings of the 2013 International Conference on Electromagnetics in Advanced Applications (ICEAA)* (IEEE, 2013), pp. 696–698.

[22] E. D. Palik, *Handbook of Optical Constants of Solids* (Elsevier, New York, 1998).

[23] P. B. Johnson and R. W. Christy, Optical constants of the noble metals, Phys. Rev. B **6**, 4370 (1972).

[24] Q. Q. Shu, Y. Jiang, S. Meng, G. Lin, and W. G. Ma, Exactly solvable model for metal–insulator–metal stepped boundary tunnel junctions, Thin Solid Films **414**, 136 (2002).

[25] P. Alonso-González, P. Albella, F. Neubrech, C. Huck, J. Chen, F. Golmar, F. Casanova, L. E. Hueso, A. Pucci, J. Aizpurua, and R. Hillenbrand, Experimental Verification of the Spectral Shift between Near- and Far-Field Peak Intensities of Plasmonic Infrared Nanoantennas, Phys. Rev. Lett. **110**, 203902 (2013).

[26] M. Jablan, H. Buljan, and M. Soljacic, Plasmonics in graphene at infrared frequencies, Phys. Rev. B **80**, 245435 (2009).

[27] K. S. Novoselov, A. K. Geim, S. V. Morozov, D. Jiang, Y. Zhang, S. V. Dubonos, I. V. Grigorieva, and A. A. Firsov, Electric field effect in atomically thin carbon films, Science **306**, 666 (2004).

[28] J.-H. Chen, C. Jang, S. Adam, M. S. Fuhrer, E. D. Williams, and M. Ishigami, Charged-impurity scattering in graphene, Nat. Phys. **4**, 377 (2008).

[29] E. H. Hwang, S. Adam, and S. Das Sarma, Transport in chemically doped graphene in the presence of adsorbed molecules, Phys. Rev. B **76**, 195421 (2007).

[30] L. Ju, J. Velasco, Jr., E. Huang, S. Kahn, C. Nosiglia, Hsin-Zon Tsai, W. Yang, T. Taniguchi, K. Watanabe, Y. Zhang, G. Zhang, M. Crommie1, A. Zettl, and F. Wang, Photoinduced doping in heterostructures of graphene and boron nitride, Nat. Nanotechnol. **9**, 348 (2014).